PROTEINS: Structure, Function, and Genetics 45:169–175 (2001)

QSAR: Hydropathic Analysis of Inhibitors of the p53–mdm2 Interaction

Peter S. Galatin and Donald J. Abraham
Department of Medicinal Chemistry and Institute for Structural Biology and Drug Discovery, Virginia Commonwealth University, Richmond, Virginia

ABSTRACT **To date, a number of p53-derived peptides have been evaluated in vitro for their ability to inhibit the carcinogenic p53–mdm2 interaction. Design of second-generation nonpeptidic compounds requires the reduction of large peptide structures down to small molecules maintaining the proper spatial arrangement of key functional groups. Molecular modeling software exists that can predict and rank intermolecular interactions from the p53–mdm2 complex crystal structure. Such analyses can yield a pharmacophore model suitable as a search query for a 3D chemical database to generate new lead compounds. As preliminary validation of this methodology, the Hydropathic INTeractions (HINT) program has been used to generate noncovalent interaction measurements between reported peptide inhibitors and mdm2. Quantitative structure–activity relationships were developed expressing peptide activity as a linear combination of hydropathic descriptors. In general, HINT measurements accurately modeled the effects of even single-atom alterations of the p53–peptide structure on activity, accounting for 70–90% of variation in experimental inhibition constants. These results surpassed those of a recently described molecular dynamics-based approach and required significantly less computation time. In conclusion, the HINT program can be integrated into the drug design cycle for next-generation p53–mdm2 complex inhibitors with confidence in its ability to simulate this noteworthy protein–protein interaction. Proteins 2001;45:169–175.**

Key words: QSAR; hydropathic; HINT; molecular modeling; drug design

INTRODUCTION

The interaction between the tumor suppressor protein p53 and the mouse double minute-2 (mdm2) oncoprotein is of significant interest in the field of molecular oncology. Although most clinically detected tumors demonstrate mutations in one or both p53 alleles, a number of cancers, particularly of the glia, bone, and soft tissues, have wild-type p53 and overexpressed mdm2.[1–7] Investigation over the last decade has shown that mdm2 inhibits p53's ability to act as a transcription factor by binding to and concealing its N-terminal transactivation domain.[8,9] Recently, a number of reports have suggested that mdm2 can also act as a ubiquitin ligase, targeting p53 for proteolytic digestion.[10–12] The x-ray crystal structure[13] of mdm2 bound to an N-terminal-derived p53 peptide presents a means for rationally designing an inhibitor of this oncogenic protein-protein interaction. The most potent inhibitors identified to date are short peptides spanning portions of the p53 transactivation domain sequence.[14] Although some of these compounds contain unnatural amino acids, they would all presumably have poor oral bioavailability and require intravenous administration. To overcome these pharmacokinetic shortcomings, the search is on for smaller nonpeptidic compounds with similar potency.[15]

One approach to generate lead compounds is to use three-dimensional (3D) chemical database searches to identify compounds able to mimic the portions of the p53 molecule crucial for binding to mdm2. An important first step of the process is defining this p53 "pharmacophore." Throughout this article, discussions of structure–activity relationships treat the p53 protein as a ligand that binds to its receptor, mdm2. Both site-directed mutagenesis and phage display have been employed to measure the effects of p53 mutation on mdm2 binding. As seen in the crystal structure, the N-terminal portion of p53 forms an amphipathic α-helix, which inserts its hydrophobic face (Phe19, Trp23, and Leu26) into a deep groove in mdm2. Much has been written about the importance of these residues, especially how mutation at even one of these positions significantly reduces the ability of p53 to bind to mdm2.[16,17]

Up to now, such experiments have guided selection of better polypeptide template structures only. There is a paucity of data that can direct the molecular paring of complete amino acid structures down to small molecule peptidomimetics. It is within this realm that molecular modeling tools have a major advantage, as one can gain insight into the possible effects of even single-atom alterations more easily in silico than in vitro. But for molecular simulation to be trusted, it is essential that computational tools be able to model existing experimental structure–function data accurately.

One computational tool in current favor for analyzing protein–protein interactions is the HINT (Hydropathic INTeractions) program (eduSoft, LC). Unlike other simula-

*Correspondence to: D.J. Abraham, Department of Medicinal Chemistry and Institute for Structural Biology and Drug Discovery, Virginia Commonwealth University, Box 980540, Richmond, VA 23298. E-mail: dabraham@hsc.vcu.edu

Received 30 January 2001; Accepted 1 June 2001

tion tools, HINT uses the empirically derived octanol: water partition coefficient fragment rules of Hansch and Leo[18] to measure the full range of electrostatic and hydrophobic interactions.[19] These are classified into favorable (hydrogen bond, acid–base, hydrophobic) and unfavorable (acid–acid, base–base, hydrophobic–polar) interactions. As solute behavior in partitioning experiments is an entropic as well as an enthalpic process, HINT calculations encode more complete thermodynamic information than do most molecular mechanics-based programs. Solvation–desolvation effects are also incorporated into the model, implicitly via the fragment constants, and explicitly by hydrophobic–polar interactions.

The total intermolecular HINT score is determined by evaluating the following formula:

$$\sum_{i=1}^{n_1}\sum_{j=1}^{n_2} a_i S_i a_j S_j T_{ij} R_{ij} + r_{ij}$$

where n_1 and n_2 are the numbers of atoms in the interacting species, a is the hydrophobic atom constant, S is the solvent accessible surface area, T is a logic function that maintains the proper sign signifying attractive or repulsive interactions, R is an interatomic distance-dependent scaling function, r is a Lennard-Jones van der Waals potential function, and i and j are indices for each pair of interacting atoms.

A host of recent publications have shown the power of HINT in quantitating protein–protein,[20,21] protein–ligand,[22–25] and protein–DNA[26,27] interactions. A few groups have performed regression analyses to relate HINT scores, whether total or by interaction class, to experimental free energy or activity (e.g., K_d or IC_{50}) values, achieving impressive cross-validated coefficients of determination in many cases.[28–30] HINT measurements have also been integrated into comparative molecular field analyses (CoMFA) and fitness functions for docking and virtual screening.[31–35]

This article presents preliminary evaluation of the HINT program for measuring the p53–mdm2 interaction and for developing predictive QSAR models for inhibitor activity. Three separate data sets are examined. The p53 mutagenesis data of Lin et al.[16] features measurements of residual mdm2 binding as a percentage of binding observed with wild-type p53.[4] Böttger et al. created a truncation series based on their best phage display-derived peptide inhibitor to map the prerequisites for activity.[36] An additional series of compounds were then synthesized by Novartis, incorporating unnatural amino acids to increase binding contacts.[14] For two of the three data sets, an r^2 value of $\geq$0.9 is achieved; the other, a function of a single hydropathic descriptor, has an r^2 value of $>$0.7. Although the data sets explored in this article are small (9, 12, and 6 compounds), the HINT program shows promise as a computational part of the drug design cycle for p53–mdm2 interaction blocking agents.

MATERIALS AND METHODS

All molecular modeling was performed on a Silicon Graphics (SGI) Indigo^2 IMPACT 10000 workstation, running IRIX version 6.5. Unless otherwise noted, software packages were utilized with default settings. Coordinate files for the p53–mdm2 complexes (human p53–human mdm2 and human p53–*Xenopus laevis* mdm2) were obtained from the Protein Data Bank[37] (www.rcsb.org) using accession codes 1YCR and 1YCQ, respectively. Protein structures were visualized with InsightII, version 98.0 (Molecular Simulations). Mutant p53 sequences were created with the InsightII Biopolymer module, which attempts to maintain as many χ side-chain torsional angles as possible in the mutant residue. Hydrogen atoms were next added to the molecule, assuming a pH of 7.4 and charged termini. For unnatural amino acid substitutions, α-aminoisobutyric acid (Aib) is an available amino acid type within InsightII, and 1-aminocyclopropanecarboxylic acid (Ac_3c) was created by forming a bond between the α-methyl groups of Aib. Phosphonomethylphenylalanine (Pmp) was formed by replacing the hydroxyl oxygen of tyrosine with carbon, adding side-chain hydrogens to make a terminal methyl group, and attaching a phosphate group so it was oriented toward Lys94 of mdm2.

To allow the protein structure to relax from the mutations, which presumably can introduce unfavorable steric or electrostatic repulsive forces, a two-step minimization process (100 steps of steepest-descent minimization, followed by conjugate-gradient minimization to an energy gradient of 0.05 kcal mol^{-1} Å^{-1}) with the CVFF force field was applied to each structure. HINT version 2.30I functions as an add-on module executed from within the InsightII program. HINT scores for the p53–mdm2 interaction of each native or mutant structure were generated as follows. First, both mdm2 and p53 were partitioned in order to assign logP values to all atoms. For mdm2, the amino acid dictionary method was employed; as the data sets for p53-related peptides include compounds containing unnatural amino acids not defined in the HINT dictionary file, p53–peptide partitions were explicitly calculated. HINT calculations employed an e^{-r} distance function with a steric term of 50. HINT table parameters restricted inter-atomic interactions to those within a distance cutoff of 6 Å and having a minimum score of 10 interaction units. HINT tables were imported into Excel 98 (Microsoft) to sort and subtotal tabulated interactions by interaction type. Partial least-squares multiple linear regression analysis with leave-one-out validation was performed using the Molecular Spreadsheet module of SYBYL version 6.5 (Tripos).

RESULTS

Generation of Human p53–mdm2 Complex With Crystallographic Waters

The 2.6-Å crystal structure of the human p53–mdm2 complex (PDB accession 1YCR) was determined by molecular replacement using the 2.3 Å *Xenopus laevis* complex structure (1YCQ) as the search model.[13] Because of its lower resolution, bound crystallographic waters for the human complex were undefined. In general, the two p53–mdm2 structures are extremely similar. Superposition of the two complexes according to a sequence align-

```
mdm2 alignment:

     21                                                    70
YCQ  EKLVQPTPLL LSLLKSAGAQ KETFTMKEVI YHLGQYIMAK QLYDEKQQHI
YCR  ETLVRPKPLL LKLLKSVGAQ KDTYTMKEVL FYLGQYIMTK RLYDEKQQHI
     25                                                    74

     71                                                   108
YCQ  VHCSNDPLGE LFGVQEFSVK EPRRLYAMIS RNLVSANV
YCR  VYCSNDLLGD LFGVPSFSVK EHRKIYTMIY RNLVV~~~
     75                                                   109

p53 alignment:

     17          27
YCQ  ETFSDLWKLL P~~
YCR  ETFSDLWKLL PEN
     17          29
```

Fig. 1. Alignments of mdm2 and p53 sequences from the two p53–mdm2 complex structures in the Protein Data Bank. For mdm2 sequences, identical residues are shaded.

Fig. 2. Superposition of two p53–mdm2 complex structures, based on 1372 atom pairs. The *Xenopus laevis* mdm2–human p53 structure is shown in white/gray; the human mdm2–human p53 structure is in red. For clarity, mdm2 is represented as a backbone ribbon trace, while p53 has all heavy atoms rendered.

ment (Fig. 1), using backbone atoms for nonconserved mdm2 residues and all atoms for conserved mdm2 and p53 residues, yielded a root-mean-square (RMS) distance of 1.39 Å over 1,372 atom pairs (Fig. 2). To approximate a solvated human p53–mdm2 complex for subsequent mutant simulations, waters from the *X. laevis* structure were then copied into the human structure.

Correlation of Partial HINT Scores With p53 Mutagenesis Data

Lin et al.[16] synthesized a large variety of mutant p53 proteins with single, double, triple, and six-site mutations in residues located in the N-terminal transcriptional activation domain.[4] Each of these mutants was compared with wild-type p53 for residual binding to the mdm2 protein through the use of immunoprecipitation experiments with radiolabeled p53 and mdm2. Table I shows the experimentally determined percentage change in mdm2 binding, as well as the changes observed in partition coefficient and HINT scores from molecular simulation. Predicted percentage change values are also listed with residual values to show the effectiveness of the model. Only mutations that were reflected in the crystal structure (residues 17–29) were modeled. In addition, the Pro27 → Tyr mutant was not modeled, as major alterations in backbone traditionally defy most prediction methodologies. The regression equation is as follows:

$$\Delta\%\ \text{mdm2 binding} = -3.857 + (12.474 \cdot \Delta \log P) - (0.285 \cdot \Delta\text{base–base}) + (0.937 \cdot \Delta\text{hydrophobic})$$

$$r^2 = 0.90,\ n = 9,\ s = 25.04,\ q^2_{\text{LOO}} = 0.76,\ P < 0.01$$

The fit of modeled to experimental data is shown in Figure 3.

Truncation Series Based on Phage-Display-Derived Peptide ^{16}MPRFMDYWEGLN^{27}

Lane et al. used an enzyme-linked immunosorbent assay (ELISA)-based format to evaluate mdm2-binding peptides discovered through phage display.[36] Briefly, microtiter plates were coated with mdm2 and probed with a combination of full-length p53 and increasing concentrations of synthetic peptides. Bound p53 was then measured with an anti-p53 antibody and enzyme-linked secondary antibody. The IC_{50} value was determined as the peptide concentration at which the peroxidase signal was one-half that of the peptide-free control. The most potent peptide reported, ^{16}MPRFMDYWEGLN^{27}, had an IC_{50} of 300 nM, compared with 9.5 μM for the wild-type sequence, ^{16}QETFSDWKLLP^{27}. To attempt to elucidate the source of the 30-fold increase of potency, a series of truncated 6–11mers of the phage-display peptide was synthesized and tested in the same assay system. Of the 27 peptides in the series, 21 spanned regions that could be completely modeled; in turn, only 12 of these had precisely determined IC_{50} values. The relevant data for these compounds is listed in Table II. Analysis of the data set yielded the following regression equation:

$$\text{pIC}_{50} = 0.455 + (0.006 \cdot \text{hydrophobic})$$

$$r^2 = 0.71,\ n = 12,\ s = 0.67,\ q^2_{\text{LOO}} = 0.59,\ P < 0.001$$

The fit of modeled to experimental data is shown in Figure 4.

Series of Peptides Including Unnatural Amino Acids

In a further round of peptide optimization, García-Echeverría et al.[14] attempted to replace residues apparently not responsible for direct p53–mdm2 contacts with α,α-disubstituted amino acids α-aminoisobutyric acid (Aib) and 1-aminocyclopropanecarboxylic acid (Ac_3c). These alterations were correctly predicted to stabilize the helical orientation of the peptide inhibitor and improve potency. In addition, the researchers recognized that the crystallographic model of the p53–mdm2 complex suggested that there were two potential avenues to incorporate additional binding contacts. First, a phosphonomethyl group was added onto Tyr22 to form a salt-bridge with Lys94 of mdm2. Also, by modifying Trp23 to a 6-chloro derivative,

TABLE I. Effect of p53 Mutation on mdm2 Binding*

Mutant	Δ%mdm2	Pred. Δ%mdm2	$\Delta HINT_{total}$	Δ*LogP*	ΔBase–base	ΔHydrophobic
Wild-type	0	−4	0	0	0	0
E17K/D21H	−20	3	−2313	4.903	366	53
L22Q	−44	−25	614	−2.934	62	35
W23S	−78	−94	−482	−1.701	180	−19
L22Q/W23S	−98	−77	−322	−4.635	13	−12
K24T	81	86	442	2.450	−58	46
L25Q/L26H	−61	−77	−286	−4.264	94	7
E28K	62	27	−811	2.655	209	61
E17K/D21H/E28K	−78	−75	−1553	7.558	684	32

*Hydropathic indices have been normalized by subtracting the relevant wild-type indices to create difference values.

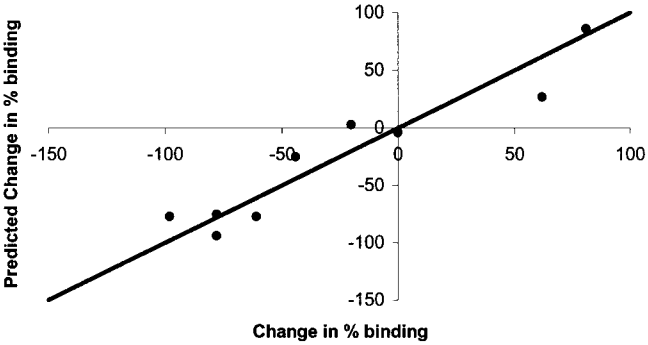

Fig. 3. Plot of predicted versus experimental percentage change in percentage binding to mdm2 for a series of full-length p53 mutants. A line of equality is drawn to show the distribution of points around a perfect correlation.

van der Waals contacts with the hydrophobic groove of mdm2 could be achieved. These approaches were validated by IC_{50} data from the aforementioned ELISA-based test, as shown in Table III.

Hydropathic descriptors allowed a high degree of prediction, as shown in the following regression equation:

$$pIC_{50} = 1.040 + (0.003 \cdot \text{hydrogen-bond}) + (0.003 \cdot \text{hydrophobic})$$

$$r^2 = 0.95,\ n = 6,\ s = 0.38,\ q^2_{LOO} = 0.81,\ P = 0.01$$

The fit of modeled to experimental data is shown in Figure 5.

DISCUSSION

Recently, Massova et al.[38] used a significantly more computationally intensive molecular dynamics (MD)-based approach to simulate the effects of p53 mutation on mdm2 binding. In what was termed "computational alanine scanning," each residue of the $p53_{16-29}$ peptide was individually mutated to alanine. The simulated free energy of binding ($\Delta G_{binding}$) of each mutated structure was subtracted from that of the native structure to yield a $\Delta\Delta G_{alanine \rightarrow X}$ for each residue. A strongly negative $\Delta\Delta G$ reflected a mutation deleterious for p53–mdm2 complex formation, a positive $\Delta\Delta G$, one favorable for binding.

In addition to their truncation series referenced above, the Lane group had also undertaken the systematic replacement of each position of their phage-display peptide with all 19 other amino acids in order to determine the number of mutations allowed (reflected by an IC_{50} increase by no more than threefold). As a demonstration of the validity of their simulation data, Massova et al., compared their $\Delta\Delta G$ values with the residue replacement data. This analysis showed overall a qualitative relationship, where residues in the wild-type human p53 sequence with highly negative $\Delta\Delta G_{alanine \rightarrow X}$ values matched up with residues in the phage-display peptide that permitted one or no mutations. Computational alanine scanning demonstrated significantly negative $\Delta\Delta G$ values for Phe19 and Trp23, but only a marginally negative score for Leu26, similar to what was seen with Leu22. None of the other residues showed significant $\Delta\Delta G$ (positive or negative). As a result, this simulation method is unable to explain, even qualitatively, striking differences in mutational tolerance, e.g., why position 16 in the phage-display peptide tolerates replacement with 18 of the 19 other amino acids, while position 21 tolerates only 5 such mutations. The simulation data of Massova et al., can be used only to suggest molecular modification on well-studied residues 19 and 23 and provides very few data on the structural requirements for the regions spanning and linking these residues.

In contrast, the HINT-based QSAR equations presented here more accurately model how a variety of structural changes large and small made to the p53 transactivation domain affect its ability to bind to mdm2. The mutant p53 proteins designed by Lin et al. were chosen to test for the effects of charge inversion (e.g., Glu → Lys) and loss of hydrophobicity (e.g., Trp → Ser). The relatively high cross-validated $r^2(q^2_{LOO})$ indicates that the hydropathic terms from the HINT model can in general predict correctly the relative contributions of p53 residues with a moderate degree of robustness. In addition to the hydrophobic residues Trp23, Leu26, and Leu22, mutations of which induced significant losses in experimental binding, two mutations (Lys24 → Thr and Glu28 → Lys) led to large increases in binding. Lin et al. do not posit any reasons why such mutations are so favorable for p53–mdm2 complex formation. In the p53–mdm2 crystal structure, Lys24 is oriented away from the intermolecular junction into bulk solvent. In agreement with this fact, the tabulated output of the HINT program does not report any interactions between Lys24 and any residue of mdm2. So how does this mutation induce such a change in the protein–

TABLE II. Phage-Display Truncation Series

Sequence	IC_{50} (μM)	pIC_{50}	Pred. pIC_{50}	$HINT_{Total}$	HH
RFMDYW	120	3.92	3.98	1048	610
PRFMDYW	40	4.40	3.72	1065	565
RFMDYWE	140	3.85	4.77	274	747
PRFMDYWE	25	4.60	4.44	101	689
RFMDYWEG	110	3.96	4.38	946	680
FMDYWEGL	2	5.70	5.82	659	928
PRFMDYWEG	150	3.82	3.91	1198	598
RFMDYWEGL	0.7	6.15	5.46	1060	866
FMDYWEGLN	13	4.89	6.08	1676	973
PRFMDYWEGL	0.1	7.00	6.19	974	992
RFMDYWEGLN	0.55	6.26	6.42	1451	1033
PRFMDYWEGLN	0.2	6.70	6.08	1458	974

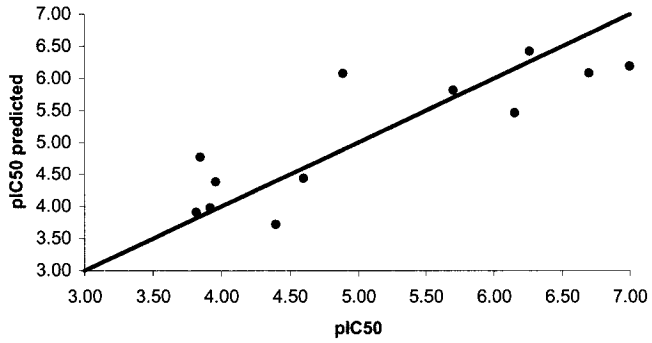

Fig. 4. Plot of predicted versus experimental pIC_{50} values for the truncation series of a phage-display-derived peptide. A line of equality is drawn to show the distribution of points around a perfect correlation.

protein interaction? Exhaustive examination of the HINT table reveals that as a result of the mutation, a number of additional hydrophobic interactions are predicted, particularly between p53 and Met62 of mdm2. Specifically, the terminal methyl group of this residue is repositioned to better interact with the backbone and side-chain atoms of Phe19 and Ser20. Furthermore, an *intra*molecular HINT calculation for the p53 peptide (data not shown) indicates that the hydroxyl group on the threonine mutation might add an additional strong hydrogen bond with the backbone oxygen of Ser20, further buttressing the helical conformation shown to be important for good binding.[14] One would think that the wild-type Lys24 could provide such a hydrogen bond. However, as the HINT table shows for the wild-type peptide, the more bulky lysine may not be able to adopt the interatomic distance and angle constraints for strong hydrogen bonding. It is interesting to note that the phage-display selected peptide reported by the Lane group contains the equivalent of a Lys24 → Glu mutation. According to the HINT intramolecular analysis, a stabilizing Glu24 ↔ Arg18 salt-bridge occurs.

Though the truncation data series was the largest studied, model building yielded the lowest cross-validated r^2 of ~0.6. It is interesting to note that such a level of prediction was achieved via a single hydropathic descriptor. At a significance level of 0.05, there are four outliers; removal of these outliers increases the r^2 from 0.71 to 0.88. In order to identify the source of the outliers, the hydrophobic interactions were separated by a participating p53 residue (Fig. 6).

As compared with the mutants of Lin et al.,[16] the peptide truncation series led to significantly divergent postminimization structures. This was reflected in the large changes in by-residue hydrophobic interaction scores that occurred between peptides with a single amino acid difference. For example, ^{18}RFMDYWE^{24} and ^{18}RFMDYWEG^{25} would appear to be extremely similar, yet the hydrophobic interaction contribution of Phe19 in the former peptide is double that of the latter. Similarly, Tyr22 maintains a fairly modest but constant contribution in all the peptides, except for ^{19}FMDYWEGL,^{26} where it is negligible. The peptides may have behaved so differently in the minimization procedure as key residues, when no longer shielded by adjacent amino acids, may have been subjected to more long-range nonbonded interactions, causing increased mobility. Although not predicted by the minimization procedure, a few of these truncations may actually lead to non-helical secondary structures. This model may not have the best statistical power, but it is far superior to one in which the minimized structure of the longest peptide, ^{17}PRFMDYWEGLN^{27} is used to compute the hydrophobic scores for all other peptides (data not shown).

The set of unnatural peptides studied by García-Echeverría et al. presents a means of evaluating HINT's recognition of more subtle changes in amino acid structure. The stabilization of the helix with the incorporation of the Ac_3c residue at position 25 also adds a hydrophobic interaction with mdm2's Leu54. HINT predicts that the phosphonomethylphenylalanine at position 22 will accept hydrogen bonds from the side-chains of Gln71, Gln72, and His73. Although acid–base contacts did not serve as a statistically significant predictor of activity, the salt-bridge between the phosphate and Lys94 is itemized in the HINT table. Addition of electron-withdrawing groups at the 6-position of Trp23 leads to additional hydrophobic contacts, as proposed by the authors. García-Echeverría et al. also observed that similar substitution at the 5-position failed to produce any changes in potency. HINT analysis of 5-Me or 5-Cl compounds shows negligible alterations in interaction scores (data not shown).

TABLE III. Peptides Containing Unnatural Amino Acids

Sequence	IC_{50} (nM)	pIC_{50}	Pred. pIC_{50}	$HINT_{Total}$	Hydrogen bond	Hydrophobic
FMDYWEGL	8949	5.05	5.25	399	214	1087
FM(Aib)YWE(Ac_3c)L	2210	5.66	5.43	−299	126	1213
FM(Aib)(Pmp)WE(Ac_3c)L	314	6.50	6.78	614	824	1037
FM(Aib)(Pmp)(6-F-Trp)E(Ac_3c)L	14	7.85	7.41	725	953	1119
FM(Aib)(Pmp)(6-Me-Trp)E(Ac_3c)L	10	8.00	8.24	1080	952	1369
FM(Aib)(Pmp)(6-CI-Trp)E(Ac_3c)L	5	8.30	8.25	1373	1040	1300

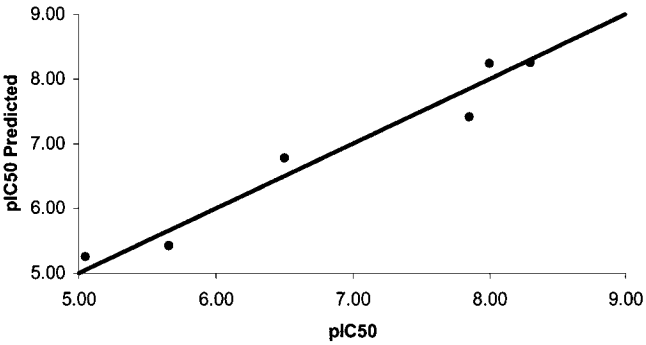

Fig. 5. Plot of predicted versus experimental pIC_{50} values for the optimization series of a phage-display-derived peptide. A line of equality is drawn to show the distribution of points around a perfect correlation.

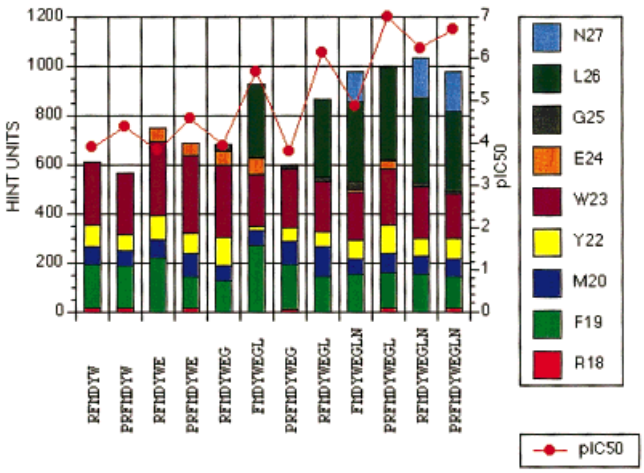

Fig. 6. Plot of hydrophobic interactions between truncated phage-display peptides and mdm2. Bar height indicates hydrophobic interaction total. The interactions for each peptide are further broken down by participating peptide residue. The experimentally determined pIC_{50} for each peptide is depicted by the superimposed line graph.

CONCLUSIONS

In conclusion, HINT interaction data can be used for correctly modeling existing experimental data describing structure–function relationships of the p53–mdm2 interaction. This preliminary validation of the HINT method provides the justification for using HINT to define essential atoms within the side-chains of Phe19, Trp23, and Leu26, a putative p53 "pharmacophore." HINT analysis of the native p53–mdm2 interaction predicts that only the terminal three carbons of the phenyl ring of Phe19 are important. Similarly, only the phenyl portion of the Trp23

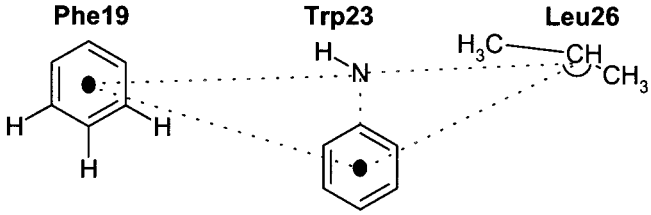

Fig. 7. Schematic of the pharmacophore for mdm2 binding, as gauged by analysis with the HINT program. All atoms displayed are explicitly entered into the 3D database searching program. The thick dots in the center of the benzene rings are centroids, the spatial average of all six-ring carbons. Dotted lines indicate distance measurements that are used as search constraints. The curved arc in Leu26 is an angle constraint.

indole side-chain along with the hydrogen-bond donor indole nitrogen is necessary. In Leu26, only the terminal side-chain isopropyl group participates in interactions. These atomic elements, the centroids defined by the phenyl rings, and the distances and angles between the atoms, are all parameters to incorporate into the 3D database search model (Fig. 7). Our future work will involve the evaluation of compounds that meet these criteria as inhibitors of the p53–mdm2 interaction.

ACKNOWLEDGMENTS

The authors thank Dr. Glen Kellogg for technical assistance with using the HINT program and Dr. James Burnett for helpful discussions.

REFERENCES

1. Momand J, Jung D, Wilczynski S, Niland J. The MDM2 gene amplification database. Nucleic Acids Res 1998;26:3453–3459.
2. Reifenberger G, Liu L, Ichimura K, Schmidt EE, Collins VP. Amplification and overexpression of the MDM2 gene in a subset of human malignant gliomas without p53 mutations. Cancer Res 1993;53:2736–2739.
3. Biernat W, Kleihues P, Yonekawa Y, Ohgaki H. Amplification and overexpression of MDM in primary (de novo) glioblastomas. J Neuropathol Exp Neurol 1997;56:180–185.
4. Oliner JD, Kinzler KW, Meltzer PS, George DL, Vogelstein B. Amplification of a gene encoding a p53-associated protein in human sarcomas. Nature 1992;358:80–83.
5. Hung J, Anderson R. p53: functions, mutations and sarcomas. Acta Orthop Scand 1997;273(suppl):68–73.
6. Lonardo F, Ueda T, Huvos AG, Healey J, Ladanyi M. p53 and MDM2 alterations in osteosarcomas: correlation with clinicopathologic features and proliferative rate. Cancer 1997;79:1541–1547.
7. Takami K, Inui H, Nagayama K, Watatani M, Yasutomi M, Kurahasi H, Mori T, Takai SI, Nishisho I. Low grade amplification of MDM2 gene in a subset of human breast cancers without p53 alterations. Breast Cancer 1994;1:95–102.
8. Momand J, Zambetti GP, Olson DC, George D, Levine AJ. The mdm-2 oncogene product forms a complex with the p53 protein

and inhibits p53-mediated transactivation. Cell 1992;69:1237–1245.
9. Thut CJ, Goodrich JA, Tjian R. Repression of p53-mediated transcription by MDM2: a dual mechanism. Gene Dev 1997;11: 1974–1986.
10. Haupt Y, Maya R, Kazaz A, Oren M. mdm2 promotes the rapid degradation of p53. Nature 1997;387:296–299.
11. Kubbutat MHG, Jones SN, Vousden KH. Regulation of p53 stability by mdm2. Nature 1997;387:299–303.
12. Fang S, Jensen JP, Ludwig RL, Vousden KH, Weissman AM. mdm2 is a RING finger-dependent ubiquitin protein ligase for itself and p53. J Biol Chem 2000;275:8945–8951.
13. Kussie PH, Gorina S, Marechal V, Elenbaas B, Moreau J, Levine AJ, Pavletich NP. Structure of the MDM2 oncoprotein bound to the p53 tumor suppressor transactivation domain. Science 1996; 274:948–953.
14. García-Echeverría C, Chène P, Blommers MJJ, Furet P. Discovery of potent antagonists of the interaction between human double minute 2 and tumor suppressor p53. J Med Chem 2000;43:3205–3208.
15. Shair MD. A closer view of an oncoprotein-tumor suppressor interaction. Chem Biol 1997;4:791–794.
16. Lin J, Chen J, Elenbaas B, Levine AJ. Several hydrophobic amino acids in the p53 amino-terminal domain are required for transcriptional activation, binding to mdm-2 and the adenovirus 5 E1B 55-kD protein. Genes Dev 1994;8:1235–1246.
17. Uesugi M, Verdine GL. The alpha-helical FXXPhiPhi motif in p53: TAF interaction and discrimination by MDM2. Proc Natl Acad Sci USA 1999;96:14801–14806.
18. Hansch C, Leo AJ. Substituent Constants for Correlation Analysis in Chemistry and Biology. New York: John Wiley & Sons; 1979.
19. Kellogg GE, Abraham DJ. Hydrophobicity: is $\log P_{o/w}$ more than the sum of its parts? Eur J Med Chem 2000;35:651–661.
20. Abraham DJ, Kellogg GE, Holt JM, Ackers GK. Hydropathic analysis of the non-covalent interactions between molecular subunits of structurally characterized hemoglobins. J Mol Biol 1997; 272:613–632.
21. Burnett JC, Kellogg GE, Abraham DJ. Computational methodology for estimating changes in free energies of biomolecular association upon mutation. The importance of bound water in dimer–tetramer assembly for beta 37 mutant hemoglobins. Biochemistry 2000;39:1622–1633.
22. Wireko FC, Kellogg GE, Abraham DJ. Allosteric modifiers of hemoglobin. 2. Crystallographically determined binding sites and hydrophobic binding/interaction analysis of novel hemoglobin oxygen effectors. J Med Chem 1991;34:758–767.
23. Kellogg GE, Joshi GS, Abraham DJ. New tools for modeling and understanding hydrophobicity and hydrophobic interactions. Med Chem Res 1992;1:444–453.
24. Wright CS, Kellogg GE. Differences in hydropathic properties of ligand binding at four independent sites in wheat germ agglutinin–oligosaccharide crystal complexes. Protein Sci 1996;5:1466–1476.
25. Wang S, Liu M, Lewin NE, Lorenzo PS, Bhattacharrya D, Qiao L, Kozikowski AP, Blumberg PM. Probing the binding of indolactam-V to protein kinase C through site-directed mutagenesis and computational docking simulations. J Med Chem 1999;42:3436–3446.
26. Kellogg GE, Scarsdale JN, Fornari FA. Identification and hydropathic characterization of structural features affecting sequence specificity for doxorubicin intercalation into DNA double-stranded polynucleotides. Nucleic Acids Res 1998;26:4721–4732.
27. Kellogg GE, Scarsdale JN, Cashman DJ. Ligand docking and scoring in DNA oligonucleotide binding of doxorubicin and modeled analogs to optimize sequence specificity. Med Chem Res 1999;9:592–603.
28. Semus SF. A novel hydropathic intermolecular field analysis (HIFA) for the prediction of ligand-receptor binding affinities. Med Chem Res 1999;9:535–547.
29. Gussio R, Pattabiraman N, Zaharevitz DW, Kellogg GE, Topol IA, Rice WG, Schaeffer CA, Erickson JW, Burt SK. All-atom models for the non-nucleoside binding site of HIV-1 reverse transcriptase complexed with inhibitors: a 3D QSAR approach. J Med Chem 1996;39:1645–1650.
30. Gussio R, Zaharevitz DW, McGrath CF, Pattabiraman N, Kellogg GE, Schultz C, Link A, Kunick C, Leost M, Meijer L, Sausville EA. Structure-based design modifications of the paullone molecular scaffold for cyclin-dependent kinase inhibition. Anticancer Drug Des 2000;15:53–66.
31. Kellogg GE, Semus SF, Abraham DJ. HINT: a new method of empirical hydrophobic field calculation for CoMFA. J Comput Aided Mol Des 1991;5:545–552.
32. Debnath AK. Three-dimensional quantitative structure-activity relationship study on cyclic urea derivatives as HIV-1 protease inhibitors: application of comparative molecular field analysis. J Med Chem 1999;42:249–259.
33. Pajeva I, Wiese M. Molecular modeling of phenothiazines and related drugs as multidrug resistance modifiers: a comparative molecular field analysis study. J Med Chem 1998;41:1815–1826.
34. Meng EC, Kuntz ID, Abraham DJ, Kellogg GE. Evaluating docked complexes with the HINT exponential function and empirical atomic hydrophobicities. J Comput Aided Mol Des 1994;8:299–306.
35. Gussio R, Pattabiraman N, Kellogg GE, Zaharevitz DW. Use of 3D QSAR methodology for data mining the National Cancer Institute repository of small molecules: application to HIV-1 reverse transcriptase inhibition. Methods 1998;14:255–263.
36. Böttger A, Böttger V, Garcia-Echevernia C, Chene P, Hochkeppel HK, Sampson W, Ang K, Howard SF, Picksley SM, Lane DP. Molecular characterization of the hdm2-p53 interaction. J Mol Biol 1997;269:744–756.
37. Berman HM, Westbrook J, Feng Z, Gilliland G, Bhat TN, Weissig H, Shindyalov IN, Bourne PE. The protein data bank. Nucleic Acids Res 2000;28:235–242.
38. Massova I, Kollman PA. Computational alanine scanning to probe protein–protein interactions: a novel approach to evaluate binding free energies. J Am Chem Soc 1999;121:8133–8143.